Information geometry aspects of minimum entropy production paths from quantum mechanical evolutions

Carlo Cafaro[1] and Paul M. Alsing[2]
[1]*SUNY Polytechnic Institute, Albany, New York 12203, USA*
[2]*Air Force Research Laboratory, Information Directorate, Rome, New York 13441, USA*

(Received 7 November 2019; revised manuscript received 16 January 2020; accepted 22 January 2020; published 10 February 2020)

We present an information geometric analysis of entropic speeds and entropy production rates in geodesic evolution on manifolds of parametrized quantum states. These pure states emerge as outputs of suitable su(2; $\mathbb{C}$) time-dependent Hamiltonian operators used to describe distinct types of analog quantum search schemes. The Riemannian metrization on the manifold is specified by the Fisher information evaluated along the parametrized squared probability amplitudes obtained from analysis of the temporal quantum mechanical evolution of a spin-1/2 particle in an external time-dependent magnetic field that specifies the su(2; $\mathbb{C}$) Hamiltonian model. We employ a minimum action method to transfer a quantum system from an initial state to a final state on the manifold in a finite temporal interval. Furthermore, we demonstrate that the minimizing (optimum) path is the shortest (geodesic) path between the two states and, in particular, minimizes also the total entropy production that occurs during the transfer. Finally, by evaluating the entropic speed and the total entropy production along the optimum transfer paths in a number of physical scenarios of interest in analog quantum search problems, we show in a clear quantitative manner that to a faster transfer there corresponds necessarily a higher entropy production rate. Thus we conclude that lower entropic efficiency values appear to accompany higher entropic speed values in quantum transfer processes.

DOI: 10.1103/PhysRevE.101.022110

I. INTRODUCTION

Riemannian geometry has been employed in a variety of different approaches in quantum searching [1,2]. In [3], it was shown that Grover's algorithm is specified by a unitary and adiabatic process that preserves the Fisher information function. In [4], the role of entanglement in quantum search was investigated in terms of the Fubini-Study metric. In [5,6], quantifying the notion of quantum distinguishability between parametric density operators by means of the Wigner-Yanase quantum information metric, it was shown that the quantum search problem can be recast in an information geometric framework wherein Grover's dynamics is characterized by a geodesic on the manifold of parametric density operators of pure quantum states constructed from the continuous approximation of the parametric quantum output state in Grover's algorithm. Finally, in Ref. [7], methods of information geometry were used to confirm the superfluity of the Walsh-Hadamard operation and, most importantly, to recover the quadratic speedup relation.

Thermodynamic perspectives on quantum computation [8] and information [9], including quantum error correction [10,11], can be quite insightful. In the framework of classical and quantum algorithms viewed in terms of simple quantum circuit models, the performance of search schemes is usually quantified by means of the query complexity of the algorithm (that is, the number of oracle queries made by the algorithm). However, more realistic models of computation should be considered to properly analyze quantum speedups. In particular, a physically realistic analysis should also take into account the thermodynamic resource costs of running these algorithms on an actual computer. Some preliminary findings are beginning to appear in the literature [12,13]. For instance, using Bennett's Brownian model of low power reversible computation [8], Perlner and Liu argued in Ref. [13] that classical exhaustive search can be quite competitive with Grover's quantum search algorithm when the comparison between the two searching schemes is made in terms of actual thermodynamic resource costs, including energy consumption, memory size, and time. The comparative analysis presented in Ref. [13] is mathematical in flavor and, most of all, focuses solely on comparing classical search schemes with Grover's quantum search algorithm. A comparison among distinct quantum searching schemes is absent in Ref. [13].

In Ref. [14], we presented an information geometric characterization of the oscillatory or monotonic behavior of statistically parametrized squared probability amplitudes emerging from special functional forms of the Fisher information function selected *ad hoc*: constant, exponential decay, and power-law decay. Furthermore, for each case, we computed both the speed and the thermodynamic divergence of the corresponding physical processes by exploiting a convenient Riemannian geometrization of useful thermodynamical concepts. Finally, we briefly discussed the possibility of employing the proposed information geometric perspective to help characterize a convenient trade-off between speed and thermodynamic efficiency in quantum search algorithms. A limitation of the work in Ref. [14] is that the Fisher information functions

were selected in an *ad hoc* fashion without specifying their emergence from a precise physical setting. Therefore, despite the mathematical generality, the observed behaviors of the parametrized squared probability amplitudes that emerged from our information geometric analysis had no obvious physical interpretation. Inspired by the work of Byrnes and collaborators [15], we presented in Ref. [16] a detailed analysis concerning the physical connection between quantum search Hamiltonians and exactly solvable time-dependent, two-level quantum systems. More specifically, we analytically calculated the transition probabilities from a source state to a target state in a number of physical scenarios characterized by a spin-1/2 particle immersed in an external time-dependent magnetic field. In particular, we investigated both the periodic oscillatory as well as the monotonic temporal behaviors of such transition probabilities and, additionally, explored their analogy with characteristic features of Grover-like and fixed-point quantum search algorithms, respectively. Finally, we discussed from a physics perspective the connection between the schedule of a search algorithm, in both adiabatic and nonadiabatic quantum mechanical evolutions, and the control magnetic fields in a time-dependent driving Hamiltonian.

In this paper, motivated by the lack of any comparative thermodynamical analysis of quantum search algorithms and building on our previous works presented in Refs. [14,16,17], we borrow the idea of Riemannian geometrization of the concepts of efficiency and speed within both quantum and thermodynamical settings in order to provide a theoretical perspective on the trade-off between speed and efficiency in terms of minimum entropy production paths emerging from quantum mechanical evolutions. Specifically, we present an information geometric analysis of entropic speeds and entropy production rates in geodesic evolution on statistical manifolds of parametrized quantum states arising as outputs of $(2;\mathbb{C})$ Hamiltonian models mimicking different types of continuous-time quantum search evolutions.

The layout of the remainder of this paper is as follows. In Sec. II, we present some preliminary information geometric concepts. Specifically, we focus our attention on the notions of Fisher information, thermodynamic length, and optimum paths. In Sec. III, we explain how the pure states that we consider emerge as outputs of suitable $\mathrm{su}(2;\mathbb{C})$ time-dependent Hamiltonian evolutions used to describe different types of analog quantum search schemes. In Sec. IV, we introduce the Riemannian metrization on the parameter manifold specified by the Fisher information evaluated along the parametrized squared probability amplitudes obtained from analysis of the temporal evolution of a spin-1/2 particle in the external time-dependent magnetic field characterizing the $\mathrm{su}(2;\mathbb{C})$ Hamiltonian model. In particular, we use a minimum action method to transfer a quantum system from an initial state to a final state on the manifold in finite time. Moreover, we demonstrate that the minimizing (optimum) path is the shortest (geodesic) path between the two states and, in particular, minimizes also the total entropy production that occurs during the transfer. Finally, by calculating the entropic speed and the total entropy production along the optimum transfer paths in a number of physical scenarios of interest in analog quantum search problems, we demonstrate in a transparent, quantitative manner that to a faster transfer there corresponds necessarily a higher entropy production rate. Finally, our concluding remarks appear in Sec. V.

II. INFORMATION GEOMETRIC PRELIMINARIES

In Sec. II, we introduce some preliminary information geometric notions. In particular, we discuss the concepts of Fisher information, thermodynamic length, and optimum paths.

A. Fisher information

From an information-theoretic perspective, the concept of Fisher information can be applied to either a multiparameter case or a single parameter case. In the former case, the Fisher information matrix $\mathcal{F}(\theta)$ with elements $\mathcal{F}_{\alpha\beta}(\theta)$ is defined as [18,19]

$$\mathcal{F}_{\alpha\beta}(\theta) \stackrel{\text{def}}{=} \sum_{x\in\mathcal{X}} p_x(\theta)\frac{\partial\,\log[p_x(\theta)]}{\partial\theta^\alpha}\frac{\partial\,\log[p_x(\theta)]}{\partial\theta^\beta}, \qquad (1)$$

where "log" denotes the natural logarithmic function. In Eq. (1), we assume X denotes a discrete random variable with alphabet $\mathcal{X}$ and probability mass function $p_X(x;\theta) = p_x(\theta)$. Furthermore, $\theta \stackrel{\text{def}}{=} (\theta^1,\ldots,\theta^M)$ with M being the dimensionality of the parameter space $\Theta \stackrel{\text{def}}{=} \{\theta\}$. The quantity $\mathcal{F}_{\alpha\beta}(\theta)$ in Eq. (1) is a measure of the minimum error in estimating a parameter θ of a distribution $p_x(\theta)$. Specifically, the Fisher information $\mathcal{F}(\theta)$ obtained from $\mathcal{F}_{\alpha\beta}(\theta)$ in Eq. (1) by assuming a one-dimensional parameter space is formally defined as the variance of the score $\mathrm{V} \stackrel{\text{def}}{=} \partial_\theta\{\log[p_x(\theta)]\}$ with $\partial_\theta \stackrel{\text{def}}{=} \partial/\partial_\theta$, $\mathcal{F}(\theta) \stackrel{\text{def}}{=} \mathrm{var}(\mathrm{V}) = E_\theta[\{\partial_\theta \log[p_x(\theta)]\}^2]$. The quantity $E_\theta[\cdot]$ denotes the expected value of the random variable V squared with respect to the probability mass function $p_x(\theta)$. We remark that the mean value of the score is zero. For the sake of convenience, we also point out that in the multiparameter case, $\mathcal{F}_{\alpha\beta}(\theta)$ in Eq. (1) can be recast as

$$\mathcal{F}_{\alpha\beta}(\theta) \stackrel{\text{def}}{=} E_\theta[(\mathrm{V}_\alpha - \langle \mathrm{V}_\alpha\rangle)(\mathrm{V}_\beta - \langle \mathrm{V}_\beta\rangle)]. \qquad (2)$$

In Eq. (2), $\langle \mathrm{V}_\alpha\rangle \stackrel{\text{def}}{=} E_\theta[\mathrm{V}_\alpha]$ and $\mathrm{V}_\alpha \stackrel{\text{def}}{=} \partial_\alpha\{\log[p_x(\theta)]\}$ with $\partial_\alpha \stackrel{\text{def}}{=} \partial/\partial\theta^\alpha$. The relevance of the Fisher information is encoded in the Cramer-Rao inequality which states that the mean-squared error of any unbiased estimator $T(X)$ of the parameter θ is lower bounded by the reciprocal of the Fisher information [18], $\mathrm{var}(T) \geqslant 1/\mathcal{F}(\theta)$. Roughly speaking, $\mathcal{F}(\theta)$ is a measure of the amount of information about θ that is present in the data and gives a lower bound on the error in estimating θ from the data.

In addition to being central to the fields of information theory [18] and information geometry [20], the concept of Fisher information plays a key role in the geometric descriptions of both quantum mechanics [21,22] and statistical mechanics [23]. For an overview of the physical meaning of the Fisher information in information theory, quantum mechanics, and thermodynamics, we refer to Table I.

B. Thermodynamic length

The Riemannian metric tensor introduced in Eq. (1) allows one to define the notions of length of a path and distance

TABLE I. Schematic description of typical fluctuating observable quantities and parameters of interest together with the physical interpretation of the concepts of Fisher information and length through parameter space in information theory, thermodynamics, and quantum theory.

Theoretical framework	Fluctuating observable quantity	Parameter of interest	Fisher information	Length
Information theory	Score function	Elapsed time	Variance of the score	Entropic
Thermodynamics	Energy	Temperature	Size of energy fluctuations	Thermodynamic
Quantum theory	Hermitian operator	Magnetic field intensity	Dispersion of the operator	Statistical

between two states in the particular state space being considered. The state space may have quantum origin or thermodynamical origin. More generally, one deals with an information-theoretic state space where states are parametrized by parameters more general than those used in thermodynamics. For these general scenarios, it is customary to define the metric tensor in terms of the information-theoretic concept of entropy where the Fisher metric tensor is employed to define a notion of distance between points in the space of parameters.

In Ref. [24], using the second derivatives of the internal energy with respect to extensive variables such as volume, Weinhold proposed a Riemannian metric in the space of thermodynamic equilibrium states. In Ref. [25], Ruppeiner presented a Riemannian geometric model of thermodynamics with a Riemann structure specified in terms of a metric tensor defined by means of second derivatives of the entropy as a function of extensive variables such as volume and mole number. In Ref. [26], Salamon and collaborators showed that Weinhold's energy version and Ruppeiner's entropy version of the thermodynamic metric tensor are conformally equivalent. Using the energy version of the thermodynamic metric tensor, Salamon and Berry defined in Ref. [27] the length of a path γ_θ with the parameter θ parametrized by an affine parameter ξ with $0 \leqslant \xi \leqslant \tau$ in the space of thermal states as

$$\mathcal{L}(\tau) \stackrel{\text{def}}{=} \int_0^\tau \sqrt{\frac{d\theta^\alpha}{d\xi} g_{\alpha\beta}(\theta) \frac{d\theta^\beta}{d\xi}}\, d\xi, \tag{3}$$

where $g_{\alpha\beta}(\theta)$ denotes the thermodynamic metric tensor. The quantity $\mathcal{L}(\tau)$ in Eq. (3) is known as the thermodynamic length of the path γ_θ and has dimensions of $(\text{energy})^{1/2}$. Clearly, it is also possible to define $\mathcal{L}(\tau)$ in terms of the entropy version of the thermodynamic metric tensor. In such a case, the corresponding "entropy" and "energy" lengths emerging from Eq. (3) will simply differ by a factor of the square root of some mean temperature during the thermodynamic process being considered [26,27]. More generally, it is also possible to show that under suitable working conditions, the entropy defined by a probability distribution leads to a length in the space of probability distributions that equals the length computed using the thermodynamic entropy in the space of extensive variables [28]. To understand the physical interpretation of the thermodynamic length, it is convenient to introduce the so-called thermodynamic divergence $\mathcal{I}(\tau)$ of a path γ_θ with the variable θ expressed in terms of an affine parameter ξ with $0 \leqslant \xi \leqslant \tau$ [29],

$$\mathcal{I}(\tau) \stackrel{\text{def}}{=} \tau \int_0^\tau \frac{d\theta^\alpha}{d\xi} g_{\alpha\beta}(\theta) \frac{d\theta^\beta}{d\xi}\, d\xi. \tag{4}$$

From Eqs. (3) and (4), using the Cauchy-Schwarz inequality, it follows that $\mathcal{I} \geqslant \mathcal{L}^2$. In particular, the equality $\mathcal{I} = \mathcal{L}^2$ is obtained only when the integrand in Eq. (4) is constant along the path γ_θ. The thermodynamic length and the thermodynamic divergence can be regarded as control measures of the dissipation of finite time thermodynamic processes. In particular, while $\mathcal{I}$ measures the number of natural fluctuations along a path, $\mathcal{L}$ is an indicator of the cumulative root-mean-square deviations measured along the path [29].

C. Optimum paths

Optimum paths γ_θ with $\theta(\xi) \stackrel{\text{def}}{=} \{\theta^\alpha(\xi)\}$, $1 \leqslant \alpha \leqslant M$, where M is the dimensionality of the parameter space, and $0 \leqslant \xi \leqslant \tau$ are paths characterized by the most favorable affine time ξ parametrization. Such a favorable time parametrization of the path $\theta(\xi)$ yields the shortest thermodynamic length. Specifically, minimization of the action functional represented by the length $\mathcal{L}$ in Eq. (3) by requiring its variation $\delta\mathcal{L}$ equals zero yields, after some straightforward tensor algebra and imposing that $\delta\theta^\alpha = 0$ at the extremum, we obtain the standard form for the geodesic equation,

$$\frac{d^2\theta^\alpha}{d\xi^2} + \Gamma^\alpha_{\beta\gamma} \frac{d\theta^\beta}{d\xi} \frac{d\theta^\gamma}{d\xi} = 0. \tag{5}$$

We note that the affine parameter ξ is not unique since it is defined up to changes of scale and origin. In summary, optimum paths are geodesic paths $\theta^\alpha(\xi)$ that solve Eq. (5). The quantities $\Gamma^\mu_{\nu\rho}$ in Eq. (5) are the Christoffel connection coefficients of the second kind defined as [30], $\Gamma^\alpha_{\beta\gamma} \stackrel{\text{def}}{=} (1/2) g^{\alpha\delta}(\partial_\beta g_{\delta\gamma} + \partial_\gamma g_{\beta\delta} - \partial_\delta g_{\beta\gamma})$ with $\partial_\beta \stackrel{\text{def}}{=} \partial/\partial\theta^\beta$. We point out that optimum paths minimizing $\mathcal{L}(\tau)$ in Eq. (3) are also paths minimizing the divergence $\mathcal{I}(\tau)$ in Eq. (4). Indeed, by minimizing $\mathcal{I}(\tau)$ under the same working assumptions employed in the minimization of the length, it can be shown after some straightforward computations that the optimum paths $\theta^\alpha(\xi)$ satisfy the equation

$$\frac{d}{d\xi}\left[\mathcal{F}_{\alpha\rho}(\theta) \frac{d\theta^\alpha}{d\xi}\right] - \frac{1}{2} \frac{d\theta^\alpha}{d\xi} \frac{\partial \mathcal{F}_{\alpha\beta}(\theta)}{\partial\theta^\rho} \frac{d\theta^\beta}{d\xi} = 0. \tag{6}$$

Interestingly, Eq. (6) is the information geometric analog of Eqs. (36) and (6) in Refs. [31] and [32], respectively. Since optimum paths are geodesic paths, the "thermodynamic" speed (henceforth, entropic speed) v_E, defined as

$$v_{\text{E}} \stackrel{\text{def}}{=} \sqrt{\frac{d\theta^\alpha}{d\xi} g_{\alpha\beta}(\theta) \frac{d\theta^\beta}{d\xi}}, \tag{7}$$

is constant when evaluated along these shortest paths. Furthermore, optimum paths are also paths that correspond to constant entropy production rate r_{E}, where r_{E} is given by

$$r_{\mathrm{E}} \stackrel{\mathrm{def}}{=} \frac{d\mathcal{I}}{d\tau}, \tag{8}$$

with $\mathcal{I}(\tau)$ defined in Eq. (4) and evaluated along the optimum paths. Finally, we point out that the entropy production rate r_{E} equals the squared invariant norm of the speed v_{E} when both quantities are evaluated along the optimum paths. For the sake of forthcoming discussions, we shall be naming lengths, divergences, and speeds as "entropic" quantities. Our proposed notion of efficiency is inspired here by the definition of thermal efficiency of a heat engine [33] and by the concept of efficiency of a quantum evolution in the Riemannian approach to quantum mechanics as presented in Ref. [34]. Specifically, replacing the condition of minimum energy dispersion with the requirement of minimum entropy production, we find it convenient to define the entropic efficiency of an evolution along a path of minimum entropic length joining the distinct initial and final points on the information manifold as

$$\eta_E \stackrel{\mathrm{def}}{=} 1 - \frac{r_E}{r}, \tag{9}$$

where $r \stackrel{\mathrm{def}}{=} \max\{\lceil r_E^{(i)} \rceil\}$ is the maximum of the ceiling functions of $r_E^{(i)} \in \mathbb{R}_+ \backslash \{0\}$ with the index "i" labeling the distinct evolutions (of quantum mechanical origin, in our case) being compared. The ceiling function maps $x \in \mathbb{R}$ to the least integer greater than or equal to x. The quantity r plays the effective role of a normalizing factor that renders η_E adimensional with $0 \leqslant \eta_E \leqslant 1$. Furthermore, in view of the fact that we wish to rank the relative entropic performance of the various evolutions, the quantity r can be interpreted as the least integer upper bound of the entropy production rate of the hottest among all cool paths available for each evolution under consideration. Clearly, the entropic efficiency η_E in Eq. (9) assumes the ideal value $\eta_E = 1$ when the evolution is characterized by a path that is maximally cooled (that is, maximally reversible). In such a case, the total entropy production remains ideally constant during the evolution and, consequently, the rate of entropy production r_E approaches the limiting value of zero.

In the next section, we describe the quantum mechanical evolutions that generate the probability paths that we use to present an information geometric analysis of speed and minimum entropy production with some of the concepts we have just introduced in the current section.

III. SU(2; $\mathbb{C}$) HAMILTONIAN MODELS

In this section, we explain the manner in which the normalized pure states that we consider emerge as outputs of suitable su(2; $\mathbb{C}$) time-dependent Hamiltonian evolutions. These normalized pure states are employed to describe, from a physics perspective, different types of analog quantum search schemes [16,17].

The quantum evolution that we consider is defined in terms of a Hamiltonian operator $\mathcal{H}_{\mathrm{su}(2;\,\mathbb{C})}$ written as the most general linear superposition of the three traceless and anti-Hermitian generators $\{i\sigma_x, -i\sigma_y, i\sigma_z\}$ of su(2; $\mathbb{C}$), the Lie algebra of the special unitary group SU(2; $\mathbb{C}$) [35], and $\mathcal{H}_{\mathrm{su}(2;\,\mathbb{C})}(t) \stackrel{\mathrm{def}}{=} a(t)(i\sigma_x) + b(t)(-i\sigma_y) + c(t)(\,i\sigma_z)$. The quantities $a(t)$, $b(t)$, and $c(t)$ are time-dependent complex coefficients, while $\vec{\sigma} \stackrel{\mathrm{def}}{=} (\sigma_x, \sigma_y, \sigma_z)$ is the Pauli vector operator [36,37]. In particular, by setting $a(t) \stackrel{\mathrm{def}}{=} -i\omega_x(t)$, $b(t) \stackrel{\mathrm{def}}{=} i\omega_y(t)$, and $c(t) \stackrel{\mathrm{def}}{=} -i\Omega(t)$, the Hamiltonian $\mathcal{H}_{\mathrm{su}(2;\,\mathbb{C})}(t)$ becomes

$$\mathcal{H}_{\mathrm{su}(2;\,\mathbb{C})}(t) \stackrel{\mathrm{def}}{=} \omega_x(t)\sigma_x + \omega_y(t)\sigma_y + \Omega(t)\sigma_z. \tag{10}$$

In the language of su(2; $\mathbb{C}$) Hamiltonian models, $\omega(t) \stackrel{\mathrm{def}}{=} \omega_x(t) - i\omega_y(t) = \omega_{\mathcal{H}}(t)e^{i\phi_\omega(t)}$ and $\Omega(t)$ denote the so-called complex transverse field and real longitudinal field, respectively. Clearly, $\omega_{\mathcal{H}}(t)$ denotes the modulus of $\omega(t)$. In what follows, we specify that longitudinal fields $\Omega(t)$ are orientedalong the z axis while transverse fields $\omega(t)$ lie in the xy plane. Considering the quantum mechanical evolution of a spin-1/2 particle (an electron, for instance) in an external time-dependent magnetic field $\vec{B}(t)$, the Hamiltonian $\mathcal{H}_{\mathrm{su}(2;\,\mathbb{C})}(t)$ in Eq. (10) can be recast as $\mathcal{H}_{\mathrm{su}(2;\,\mathbb{C})}(t) \stackrel{\mathrm{def}}{=} -\vec{\mu}\cdot\vec{B}(t)$, where $\vec{\mu} \stackrel{\mathrm{def}}{=} (e\hbar/2mc)\vec{\sigma}$ is the magnetic moment of the electron with $\mu_{\mathrm{Bohr}} \stackrel{\mathrm{def}}{=} e\hbar/(2mc)$ denoting the so-called Bohr magneton. The quantity m denotes the mass of an electron, while $|e|$ is the absolute value of the electric charge of an electron. Furthermore, c and $\hbar$ denote the speed of light and the reduced Planck constant, respectively. The magnetic field $\vec{B}(t)$ can be decomposed as $\vec{B}(t) \stackrel{\mathrm{def}}{=} \vec{B}_\perp(t) + \vec{B}_\parallel(t)$, with $\vec{B}_\perp(t) \stackrel{\mathrm{def}}{=} B_x(t)\hat{x} + B_y(t)\hat{y}$ and $\vec{B}_\parallel(t) \stackrel{\mathrm{def}}{=} B_z(t)\hat{z}$. It is straightforward to identify the link between the set of field intensities $\{\omega_{\mathcal{H}}(t), \Omega_{\mathcal{H}}(t)\}$ and the set of magnetic field intensities $\{B_\perp(t), B_\parallel(t)\}$. In particular, we note that $B_\perp(t) \propto \omega_{\mathcal{H}}(t)$ and $B_\parallel(t) \propto \Omega_{\mathcal{H}}(t) \stackrel{\mathrm{def}}{=} |\Omega(t)|$. In terms of components, the exact relation between $\{B_x(t), B_y(t), B_z(t)\}$ and $\{\omega_x(t), \omega_y(t), \Omega(t)\}$ is given by $B_x(t) = -(2mc/e\hbar)\omega_x(t)$, $B_y(t) = -(2mc/e\hbar)\omega_y(t)$, and $B_z(t) = -(2mc/e\hbar)\Omega(t)$. Furthermore, in terms of field intensities, we obtain $B_\perp(t) = (2mc/|e|\hbar)\omega_{\mathcal{H}}(t)$ and $B_\parallel(t) = (2mc/|e|\hbar)\Omega_{\mathcal{H}}(t)$. Investigating the quantum mechanical evolution of an electron specified by the Hamiltonian $\mathcal{H}_{\mathrm{su}(2;\,\mathbb{C})}(t)$ in terms of exact analytical expressions of complex probability amplitudes and/or real transition probabilities from an initial source state to a final target state is a highly nontrivial matter. The unitarity of the quantum mechanical evolution requires that the complex probability amplitudes $\alpha(t)$ and $\beta(t)$ satisfy the normalization condition, $|\alpha(t)|^2 + |\beta(t)|^2 = 1$. Given the unitary evolution operator $\mathcal{U}(t)$ with $i\hbar\dot{\mathcal{U}}(t) = \mathcal{H}_{\mathrm{su}(2;\,\mathbb{C})}\mathcal{U}(t)$ and $\dot{\mathcal{U}} \stackrel{\mathrm{def}}{=} \partial_t\mathcal{U}$, the temporal evolution of a quantum source state $|s\rangle \stackrel{\mathrm{def}}{=} x|w\rangle + \sqrt{1-x^2}|w_\perp\rangle$ can be specified by means of the mapping, $(x, \sqrt{1-x^2}) \to [\alpha(t)x + \beta(t)\sqrt{1-x^2},\ -\beta^*(t)x + \alpha^*(t)\sqrt{1-x^2}]$, where $x \stackrel{\mathrm{def}}{=} \langle w|s\rangle$ is the quantum overlap. The set of orthonormal state vectors $\{|w\rangle, |w_\perp\rangle\}$ span the two-dimensional search space of the $N = 2^n$-dimensional complex Hilbert space $\mathcal{H}_2^n$. Therefore, the probability that the source state $|s\rangle$ transitions

TABLE II. Schematic description of the complex transverse field $\omega(t)$, the resonance condition in terms of the longitudinal magnetic field intensity $B_{\parallel}(t)$, and the transverse magnetic field intensity $B_{\perp}(t)$ in the chosen four quantum mechanical Rabi scenarios.

Rabi scenario	Tranversal magnetic field intensity, $B_{\perp}(t)$	Resonance condition	Complex tranverse field, $\omega(t)$
Original	$\frac{2mc}{\lvert e\rvert\hbar}\Gamma$	$B_{\parallel} = \frac{mc}{e}\omega_0$	$\Gamma\, e^{i\phi_\omega(t)}$
Generalized	$\frac{2mc}{\lvert e\rvert\hbar}\omega_{\mathcal{H}}(t)$	$B_{\parallel}(t) = \frac{mc}{e}\dot{\phi}_\omega(t)$	$\Gamma\, \cos(\lambda t) e^{i\phi_\omega(t)}$
Generalized	$\frac{2mc}{\lvert e\rvert\hbar}\omega_{\mathcal{H}}(t)$	$B_{\parallel}(t) = \frac{mc}{e}\dot{\phi}_\omega(t)$	$\frac{\Gamma}{(1+\lambda t)^2} e^{i\phi_\omega(t)}$
Generalized	$\frac{2mc}{\lvert e\rvert\hbar}\omega_{\mathcal{H}}(t)$	$B_{\parallel}(t) = \frac{mc}{e}\dot{\phi}_\omega(t)$	$\Gamma\, e^{-\lambda t} e^{i\phi_\omega(t)}$

into the target state $|w\rangle$ under $\mathcal{U}(t)$ is given by

$$\begin{aligned}\mathcal{P}_{|s\rangle\to|w\rangle}(t) &\stackrel{\text{def}}{=} |\langle w|\mathcal{U}(t)|s\rangle|^2 \\ &= |\alpha(t)|^2 x^2 + |\beta(t)|^2(1-x^2) \\ &\quad + [\alpha(t)\beta^*(t) + \alpha^*(t)\beta(t)]x\sqrt{1-x^2}. \quad (11)\end{aligned}$$

It is clear from Eq. (11) that, in orderto compute the exact analytical expression of transition probabilities, one needs to have the exact analytical expression of the evolution operator $\mathcal{U}(t)$ in terms of the complex probability amplitudes $\alpha(t)$ and $\beta(t)$.

Following our previous work presented in Ref. [16] and exploiting the results in Refs. [38,39], we consider here four quantum mechanical scenarios in which the transition probability $\mathcal{P}_{|w_\perp\rangle\to|w\rangle}(t)$ from an initial state $|w_\perp\rangle$ to a final state $|w\rangle$, where $\langle w_\perp|w\rangle = \delta_{w_\perp,w}$ and with $\sigma_z|w\rangle = +|w\rangle$ and $\sigma_z|w_\perp\rangle = -|w_\perp\rangle$, can be expressed in an exact analytical manner. In all four cases, we assume to be in a physical situation where $\dot{\phi}_\omega(t) = \omega_0$, $\Omega(t) = -\frac{\hbar}{2}\omega_0$, and ω_0 is a negative constant. We emphasize that, from a formal mathematical viewpoint, more general temporal behaviors of $\dot{\phi}_\omega(t)$ and $\Omega(t)$ could have been chosen provided the so-called generalized Rabi condition as presented in Refs. [38,39], $\dot{\phi}_\omega(t) + (2/\hbar)\Omega(t) = 0$, is satisfied. However, the choice made appears to be more convenient from an experimental perspective.

The four scenarios can be formally distinguished by means of the temporal expression of the field intensity $\omega_{\mathcal{H}}(t)$. In the first case, we assume a constant field intensity $\omega_{\mathcal{H}}(t)$, $\omega^{(1)}_{\mathcal{H}}(t) \stackrel{\text{def}}{=} \Gamma$. This case defines the original Rabi scenario where $\mathcal{P}_{|w_\perp\rangle\to|w\rangle}(t)$ is given by $\mathcal{P}^{(1)}_{|w_\perp\rangle\to|w\rangle}(t) = \sin^2[(\Gamma/\hbar)t]$. In the remaining three cases, we consider three generalized Rabi scenarios where the field intensity $\omega_{\mathcal{H}}(t)$ exhibits oscillatory, power law decay, and exponential law decay behaviors, $\omega^{(2)}_{\mathcal{H}}(t) \stackrel{\text{def}}{=} \Gamma\, \cos(\lambda t)$, $\omega^{(3)}_{\mathcal{H}}(t) \stackrel{\text{def}}{=} \frac{\Gamma}{(1+\lambda t)^2}$, and $\omega^{(4)}_{\mathcal{H}}(t) \stackrel{\text{def}}{=} \Gamma\, e^{-\lambda t}$, respectively. Observe that $\omega^{(2)}_{\mathcal{H}}(t)$ is a positive quantity on a temporal scale with $0 \leqslant t \leqslant (\pi/2)\lambda^{-1}$. In all three cases, it can be shown that the transition probability $\mathcal{P}^{(j)}_{|w_\perp\rangle\to|w\rangle}(t)$ is given by [39]

$$\mathcal{P}^{(j)}_{|w_\perp\rangle\to|w\rangle}(t) = \sin^2\left[\int_0^t \frac{\omega^{(j)}_{\mathcal{H}}(t')}{\hbar}dt'\right], \quad (12)$$

for any $j \in \{2,3,4\}$. Interestingly, being on resonance, the transition probability in all four cases depends only on the integral of the transverse field intensity $\omega_{\mathcal{H}}(t)$. In this paper, the chosen expressions of $\omega_{\mathcal{H}}(t)$ serve to specify the particular type of behavior of the analog quantum search algorithms that correspond to the time-dependent two-level quantum systems, the latter being characterized by the selected transverse field intensity.

A summary of the main properties of the four quantum evolutions that we consider in this paper appear in Table II. The transition probabilities $\mathcal{P}^{(k)}_{|w_\perp\rangle\to|w\rangle}(t)$ with $1 \leqslant k \leqslant 4$ are the essential quantities that we use to construct our parametrized output quantum states in the next section.

IV. OPTIMUM PATHS, ENTROPIC SPEED, AND ENTROPY PRODUCTION RATE

In this section, we first introduce the Riemannian metrization on the parameter manifold specified by the Fisher information [see Eq. (1)] introduced in Sec. II evaluated along the parametrized squared probability amplitudes obtained from the analysis of the temporal evolution of a spin-1/2 particle in an external time-dependent magnetic field that characterizes the su(2; $\mathbb{C}$) Hamiltonian model described in Sec. III. Then, using a minimum action method to transfer a quantum system from an initial state to a final state on the manifold in finite time, we show that the minimizing (optimum) path is the shortest (geodesic) path between the two states, and, in particular, minimizes also the total entropy production that occurs during the transfer. Finally, by calculating the entropic speed [see Eq. (7)] and the entropy production rate [see Eq. (8)] along the optimum transfer paths in the physical scenarios outlined in Sec. III and Table II, we verify in a transparent quantitative manner that to a faster transfer there corresponds necessarily a higher entropy production rate.

A. From quantum evolutions to probability paths

In our work, the parameter θ denotes the statistical version of the elapsed time t where we assume that θ is an experimental parameter that can be determined by measurement of a conventional observable that varies with time [for instance, the transverse magnetic field intensity $B_\perp(t) = (2mc/|e|\hbar)\omega_{\mathcal{H}}(t)$]. We point out that choosing the elapsed time as the experimentally controllable statistical parameter is not unusual. For example, the comparison between the inverse temperature $\beta \stackrel{\text{def}}{=} (k_B T)^{-1}$ with k_B denoting the Boltzmann constant and $\theta/\hbar$ is reminiscent of the well-known connection between statistical mechanics and quantum mechanics in terms of the so-called Wick rotation. Specifically, by replacing β with the imaginary time $it/\hbar$, the Wick rotation allows one to compute quantum mechanical probability amplitudes just as one calculates averages of observables in statistical mechanics. Therefore, by minimizing the entropy production, we shall find the optimum paths on the manifold of state space parametrized by θ along which one drives

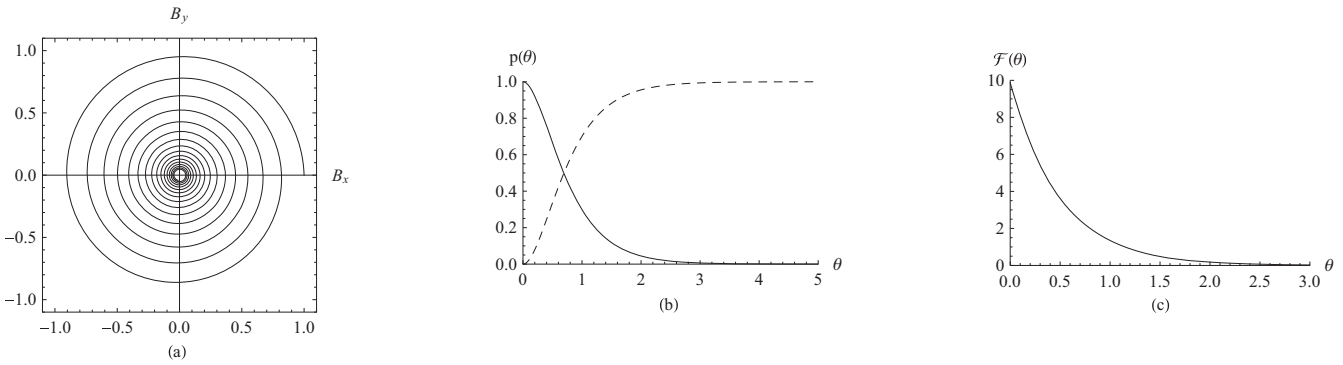

FIG. 1. Illustrative depiction of the behavior of the Fisher information $\mathcal{F}(\theta)$ versus θ [plot (c)] defined in terms of the transition probabilities $p_w(\theta)$ (dashed line) and $p_{w_\perp}(\theta)$ (solid line) [plot (b)]. These probabilities, in turn, emerge from the specific external magnetic field configuration $\vec{B} = \vec{B}_\perp + \vec{B}_\parallel$ with $\vec{B}_\perp = B_x\hat{x} + B_y\hat{y}$ [plot (a)] that characterizes the su(2; $\mathbb{C}$) Hamiltonian model being considered. In plots (b) and (c), we set $\Gamma/\hbar\lambda = \pi/2$ and $\lambda = 1$. In plot (a), the two-dimensional parametric plot of the transverse magnetic field components, we set $|\omega_0| = 10\pi$ and $\lambda = 1$. Furthermore, for simplifying normalization purposes, we also set $\Gamma/\mu_{\text{Bohr}} = 1$ with μ_{Bohr} denoting the Bohr magneton in plot (a). All physical quantities are assumed to be suitably expressed in terms of the MKSA unit system. Finally, the su(2; $\mathbb{C}$) Hamiltonian model considered in this figure corresponds to the fourth scenario studied in the paper.

the system. To be more specific, in view of the connection between analog quantum search and two-level quantum systems [16,17], we assume that the output of a continuous-time quantum search algorithm where the input is the normalized $N = 2^n$-dimensional n-qubit source state $|s\rangle \stackrel{\text{def}}{=} |\psi(\theta_0)\rangle$ can be described as $|\psi(\theta)\rangle \stackrel{\text{def}}{=} e^{i\varphi_w(\theta)}\sqrt{p_w(\theta)}|w\rangle + e^{i\varphi_{w_\perp}(\theta)}\sqrt{p_{w_\perp}(\theta)}|w_\perp\rangle$. The N-dimensional normalized output state $|\psi(\theta)\rangle$ belongs to the two-dimensional subspace of the n-qubit complex Hilbert space $\mathcal{H}_2^n$ spanned by the set of orthonormal state vectors $\{|w\rangle, |w_\perp\rangle\}$ and containing the source state $|s\rangle$. The squared probability amplitude $p_w(\theta) \stackrel{\text{def}}{=} |\langle w|\psi(\theta)\rangle|^2$ and $p_{w_\perp}(\theta) \stackrel{\text{def}}{=} |\langle w_\perp|\psi(\theta)\rangle|^2$ denote the success and failure probabilities of the search algorithm, respectively. Finally, $\varphi_w(\theta)$ and $\varphi_{w_\perp}(\theta)$ are real quantum phases of the states $|w\rangle$ and $|w_\perp\rangle$, respectively. The quantum state $|\psi(\theta)\rangle$ is parametrized in terms of a single continuous real parameter that emerges from the (computing) elapsed time of the algorithm. As briefly mentioned earlier, this parameter θ plays the role of a statistical macrovariable used to distinguish neighboring quantum states $|\psi(\theta)\rangle$ and $|\psi(\theta)\rangle + |d\psi(\theta)\rangle$ along a path through the space of quantum mechanical pure states. In summary, given our working conditions outlined earlier and assuming to have $|\psi(\theta_0)\rangle = |w_\perp\rangle$ as our input state, we shall essentially focus on the space of probability distributions $\{p(\theta)\}$ with $p(\theta) \stackrel{\text{def}}{=} (p_w(\theta), p_{w_\perp}(\theta))$ and with the natural Riemannian distinguishability metric given by the Fisher information metric in Eq. (1) (which, under suitably chosen working conditions [22], can be taken proportional to the Fubini-Study metric), $|\psi(\theta)\rangle \mapsto p(\theta) = (p_w(\theta), p_{w_\perp}(\theta)) = (|\langle w|\psi(\theta)\rangle|^2, |\langle w_\perp|\psi(\theta)\rangle|^2)$. In Fig. 1, we report the behavior of the Fisher information evaluated along the probabilities obtained from an su(2; $\mathbb{C}$) quantum evolution specified by an exponentially decaying transverse field intensity $\omega_{\mathcal{H}}^{(4)}(t)$.

B. Illustrative examples

In order to compute the entropic speed v_{E} and the entropy production rate r_{E} along the optimum cooling paths, we clearly need to first locate such paths. The expression of paths γ_θ with $\theta = \theta(\xi)$ and ξ being an affine parameter depends upon the specific parametric behavior of the Fisher information $\mathcal{F}(\theta) = E_\theta[\{\partial_\theta \log[p_x(\theta)]\}^2]$ evaluated along the probability paths $p(\theta) \stackrel{\text{def}}{=} (p_w(\theta), p_{w_\perp}(\theta))$. The probabilities $p_w(\theta)$ and $p_{w_\perp}(\theta)$ emerge, in turn, from analyzing the chosen Schrödinger evolutions specified in the previous subsection. Therefore, the Fisher information plays a key role in our proposed information geometric analysis of quantum mechanical evolutions.

1. Constant Fisher information

In the first quantum mechanical scenario that we consider, the space of probability distributions $\{p(\theta)\}$ with $p(\theta) \stackrel{\text{def}}{=} (p_w(\theta), p_{w_\perp}(\theta))$ is defined in terms of the success and failure probabilities

$$p_w(\theta) \stackrel{\text{def}}{=} \sin^2\left(\frac{\Gamma}{\hbar}\theta\right), \quad p_{w_\perp}(\theta) \stackrel{\text{def}}{=} \cos^2\left(\frac{\Gamma}{\hbar}\theta\right), \tag{13}$$

respectively. We note that the probabilities in Eq. (13) exhibit a periodic oscillatory behavior with period given by $T \stackrel{\text{def}}{=} (\pi\hbar)/\Gamma$. Using Eq. (13), the Fisher information $\mathcal{F}(\theta)$ in Eq. (1) becomes a constant quantity $\mathcal{F}_0$ with $\mathcal{F}(\theta) = \mathcal{F}_0 \stackrel{\text{def}}{=} 4(\Gamma/\hbar)^2$. Furthermore, since we are focusing on a single parameter probability path γ_θ with $\theta = \theta(\xi)$, the geodesic equations in Eq. (6) reduce to

$$\frac{d^2\theta}{d\xi^2} + \frac{1}{2\mathcal{F}}\frac{d\mathcal{F}}{d\theta}\left(\frac{d\theta}{d\xi}\right)^2 = 0. \tag{14}$$

In particular, given that $\mathcal{F}(\theta) = \mathcal{F}_0$, Eq. (14) yields $d^2\theta/d\xi^2 = 0$. Assuming nonvanishing positive initial conditions $\theta(\xi_0) = \theta_0$ and $\dot{\theta}(\xi_0) = \dot{\theta}_0$, integration of the geodesic equation is trivial and leads to the following optimum paths:

$$\theta(\xi) = \theta_0 + \dot{\theta}_0(\xi - \xi_0). \tag{15}$$

From the knowledge of the optimum paths, we can finally compute both the entropic speed v_{E} and the entropy

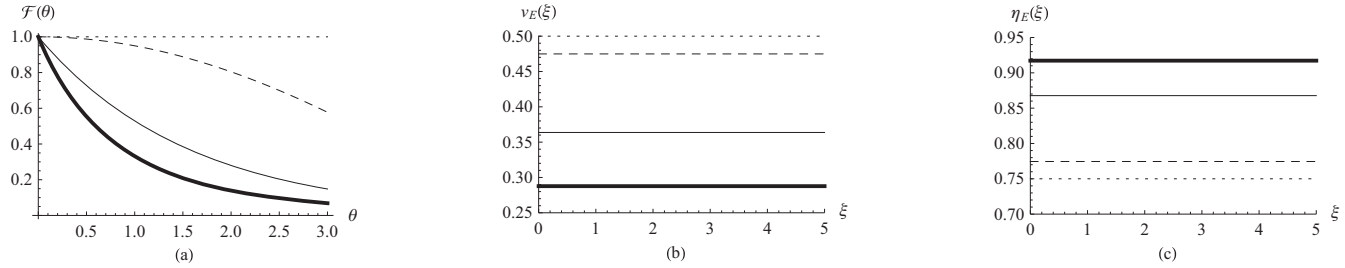

FIG. 2. Illustrative depiction of the behavior of the Fisher information $\mathcal{F}(\theta)$ versus θ [plot (a)], the entropic speed $v_E(\xi)$ versus ξ [plot (b)], and the entropic efficiency $\eta_E(\xi)$ versus ξ [plot (c)]. Dotted, dashed, thin solid, and thick solid lines in plots (a), (b), and (c) correspond to constant, oscillatory, exponential decay, and power law decay of the Fisher information, respectively. In all plots, we impose $\Gamma/(\hbar\lambda) = \pi/2$, $\lambda = 1/\pi$, $\theta_0 = 1$, and $\dot{\theta}_0 = 1$. Finally, all physical quantities are assumed to be suitably expressed in terms of the MKSA unit system.

production rate $r_{\rm E}$ that characterize the geodesic motion on the statistical manifold being considered. Specifically, evaluating the entropic speed $v_{\rm E}$ in Eq. (7) and the total entropy production $r_{\rm E}$ in Eq. (4) along the optimum paths in Eq. (15), we obtain

$$v_{\rm E}(\Gamma) = \frac{\Gamma}{\hbar}\dot{\theta}_0, \quad r_{\rm E}(\Gamma) = \left(\frac{\Gamma}{\hbar}\right)^2 \dot{\theta}_0^2, \tag{16}$$

respectively. From Eq. (16), we note that $v_{\rm E}(\Gamma) \propto \Gamma$, while $r_{\rm E}(\Gamma) \propto \Gamma^2$. Therefore, the magnitude $\omega_{\mathcal{H}}^{(1)}(t) = \Gamma$ of the complex transverse field that specifies the su(2; $\mathbb{C}$) Hamiltonian in Eq. (10) is the essential quantity that one needs to manipulate in order to find a convenient tradeoff between speed and entropy production rate within our information geometric analysis of quantum mechanical evolutions.

2. *Oscillatory behavior of the Fisher information*

In the second quantum mechanical scenario that we analyze, the space of probability distributions $\{p(\theta)\}$ with $p(\theta) \stackrel{\rm def}{=} (p_w(\theta), p_{w_\perp}(\theta))$ is defined in terms of the success and failure probabilities

$$p_w(\theta) \stackrel{\rm def}{=} \sin^2\left[\frac{\Gamma}{\hbar\lambda}\sin(\lambda\theta)\right],$$
$$p_{w_\perp}(\theta) \stackrel{\rm def}{=} \cos^2\left[\frac{\Gamma}{\hbar\lambda}\sin(\lambda\theta)\right], \tag{17}$$

respectively. From Eq. (17), we observe that the probabilities $p_w(\theta)$ and $p_{w_\perp}(\theta)$ exhibit a periodic oscillatory behavior with period given by $T \stackrel{\rm def}{=} \pi/\lambda$. In particular, $p_w(\theta)$ reaches its maximum value $\sin^2[\Gamma/(\hbar\lambda)]$ at $t^* \stackrel{\rm def}{=} \pi/(2\lambda)$. Therefore, in order for $p_w(\theta)$ to reach a maximum value equal to one, we need to impose the constraint $\Gamma = (h/4)\lambda$. Employing Eq. (17), the Fisher information $\mathcal{F}(\theta)$ becomes $\mathcal{F}(\theta) = 4(\Gamma/\hbar)^2\cos^2(\lambda\theta)$. In the case being considered, Eq. (14) becomes $d^2\theta/d\xi^2 - \lambda\tan(\lambda\theta)(d\theta/d\xi)^2 = 0$. Assuming nonvanishing positive initial conditions $\theta(\xi_0) = \theta_0$ and $\dot{\theta}(\xi_0) = \dot{\theta}_0$, integration of the geodesic equation yields optimum paths $\theta(\xi)$, whose general expression can be recast as

$$\theta(\xi) = \theta_0 + \frac{\sqrt{1-\lambda^2\xi_0^2}}{\lambda}\dot{\theta}_0[\sin^{-1}(\lambda\xi) - \sin^{-1}(\lambda\xi_0)]. \tag{18}$$

From the knowledge of the optimum paths, we can find both the entropic speed $v_{\rm E}$ and the entropy production rate $r_{\rm E}$ that specify the geodesic motion on the statistical manifold being considered. Specifically, evaluating the entropic speed $v_{\rm E}$ in Eq. (7) and the total entropy production $r_{\rm E}$ in Eq. (4) along the optimum paths in Eq. (18), we find

$$v_{\rm E}(\Gamma) = \frac{\Gamma}{\hbar}|\cos(\lambda\theta_0)|\dot{\theta}_0, \quad r_{\rm E}(\Gamma) = \left(\frac{\Gamma}{\hbar}\right)^2 \cos^2(\lambda\theta_0)\dot{\theta}_0^2, \tag{19}$$

respectively. Comparing Eqs. (19) and (16), we note that with respect to the first scenario, this second scenario is characterized by a geodesic motion generating cooler optimum paths explored with a smaller entropic speed.

3. *Power law decay of the Fisher information*

In the third quantum mechanical scenario that we investigate, the space of probability distributions $\{p(\theta)\}$ with $p(\theta) \stackrel{\rm def}{=} (p_w(\theta), p_{w_\perp}(\theta))$ is specified by means of the success and failure probabilities

$$p_w(\theta) \stackrel{\rm def}{=} \sin^2\left[\frac{\Gamma}{\hbar\lambda}\left(1 - \frac{1}{1+\lambda\theta}\right)\right],$$
$$p_{w_\perp}(\theta) \stackrel{\rm def}{=} \cos^2\left[\frac{\Gamma}{\hbar\lambda}\left(1 - \frac{1}{1+\lambda\theta}\right)\right], \tag{20}$$

respectively. The probability $p_w(\theta)$ in Eq. (20) exhibits an asymptotic monotonic convergence to one provided that $\Gamma = (h/4)\lambda$. Furthermore, making use of Eq. (20), the Fisher information $\mathcal{F}(\theta)$ becomes $\mathcal{F}(\theta) = 4(\Gamma/\hbar)^2(1+\lambda\theta)^{-4}$. In this case, Eq. (14) can be expressed as $d^2\theta/d\xi^2 - [2\lambda/(1+\lambda\theta)](d\theta/d\xi)^2 = 0$. Assuming nonvanishing positive initial conditions $\theta(\xi_0) = \theta_0$ and $\dot{\theta}(\xi_0) = \dot{\theta}_0$ and integrating this geodesic equation, the optimum paths become

$$\theta(\xi) = \frac{(1+\lambda\theta_0)^2 + \lambda\dot{\theta}_0\left[(\xi-\xi_0) - \frac{1+\lambda\theta_0}{\lambda\dot{\theta}_0}\right]}{\lambda^2\dot{\theta}_0\left[\frac{1+\lambda\theta_0}{\lambda\dot{\theta}_0} - (\xi-\xi_0)\right]}. \tag{21}$$

Once again, from the knowledge of the optimum paths, we can calculate both the entropic speed and the entropy production rate that characterize the geodesic motion on the statistical manifold being considered. Specifically, evaluating the entropic speed $v_{\rm E}$ in Eq. (7) and the entropy production rate $r_{\rm E}$

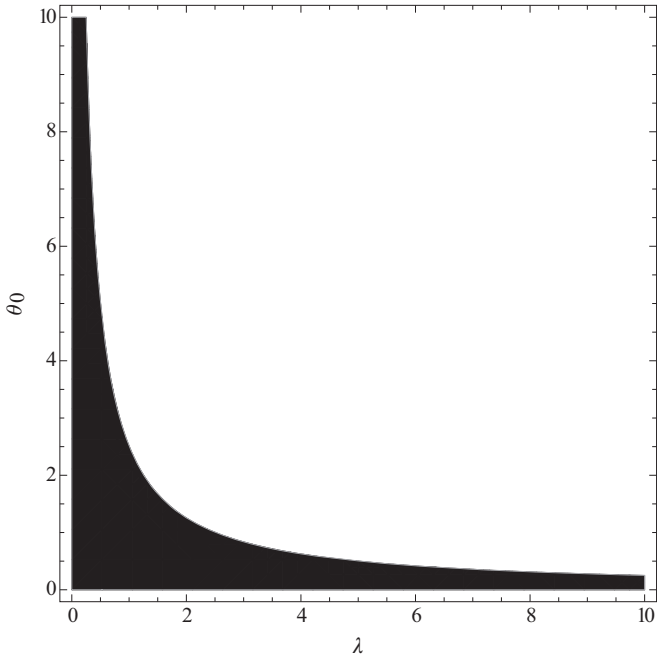

FIG. 3. Plot of the two-dimensional parametric region $\mathcal{P}$ where the exponential decay strategy outperforms the power law decay strategy in terms of higher entropic speed values. The black region $\mathcal{P}$ tends to vanish as the values of λ become sufficiently large.

in Eq. (8) along the optimum paths in Eq. (21), we obtain

$$v_{\mathrm{E}}(\Gamma) = \frac{\Gamma}{\hbar}\frac{1}{[1+\lambda(\Gamma)\theta_0]^2}\dot{\theta}_0,$$
$$r_{\mathrm{E}}(\Gamma) = \left(\frac{\Gamma}{\hbar}\right)^2\frac{1}{[1+\lambda(\Gamma)\theta_0]^4}\dot{\theta}_0^2, \tag{22}$$

respectively, where $\lambda(\Gamma) \stackrel{\mathrm{def}}{=} (4\Gamma)/h$. In analogy to the first and second scenarios, the motion on the manifold associated with the third scenario proceeds at constant entropic speed v_{E} and, thus, exhibits minimum entropy production. In particular, this third scenario is characterized by a geodesic motion that yields optimum paths cooler than those found in the second scenario.

4. Exponential decay of the Fisher information

In the fourth and last quantum mechanical scenario that we analyze, the space of probability distributions $\{p(\theta)\}$ with $p(\theta) \stackrel{\mathrm{def}}{=} (p_w(\theta), p_{w_\perp}(\theta))$ is defined in terms of the success and failure probabilities

$$p_w(\theta) \stackrel{\mathrm{def}}{=} \sin^2\left[\frac{\Gamma}{\hbar\lambda}(1-e^{-\lambda\theta})\right],$$
$$p_{w_\perp}(\theta) \stackrel{\mathrm{def}}{=} \cos^2\left[\frac{\Gamma}{\hbar\lambda}(1-e^{-\lambda\theta})\right], \tag{23}$$

respectively. The probability $p_w(\theta)$ in Eq. (23) exhibits an asymptotic monotonic convergence to one provided that $\Gamma = (h/4)\lambda$. Moreover, using Eq. (23), the Fisher information $\mathcal{F}(\theta)$ becomes $\mathcal{F}(\theta) = 4(\Gamma/\hbar)^2 e^{-2\lambda\theta}$. In this case, the geodesic equation becomes $d^2\theta/d\xi^2 - \lambda(d\theta/d\xi)^2 = 0$. Considering nonvanishing positive initial conditions $\theta(\xi_0) = \theta_0$ and $\dot{\theta}(\xi_0) = \dot{\theta}_0$, integration of the geodesic equation yields the following optimum paths:

$$\theta(\xi) = \theta_0 - \frac{1}{\lambda}\log[1-\lambda\dot{\theta}_0(\xi-\xi_0)]. \tag{24}$$

As pointed out in the previous illustrative examples, from the knowledge of the optimum paths, we can determine both the entropic speed v_{E} and the entropy production rate r_{E} that characterize the geodesic motion on the statistical manifold under consideration. Specifically, evaluating the entropic speed v_{E} in Eq. (7) and the total entropy production in Eq. (4) along the optimum paths in Eq. (24), we find

$$v_{\mathrm{E}}(\Gamma) = \frac{\Gamma}{\hbar}e^{-\lambda(\Gamma)\theta_0}\dot{\theta}_0, \quad r_{\mathrm{E}}(\Gamma) = \left(\frac{\Gamma}{\hbar}\right)^2 e^{-2\lambda(\Gamma)\theta_0}\dot{\theta}_0^2, \tag{25}$$

respectively, where $\lambda(\Gamma) \stackrel{\mathrm{def}}{=} (4\Gamma)/h$. From the comparison of Eqs. (22) and (25), we conclude that this last scenario can exhibit the coolest optimum paths, albeit with the path exploration occurring at the slowest entropic speed for values of $\lambda(\Gamma)$ sufficiently large. More specifically, we observe that $0 \leqslant e^{-\lambda\theta_0} \leqslant 1/(1+\lambda\theta_0)^2 \leqslant |\cos(\lambda\theta_0)| \leqslant 1$ when $\theta_0 \in \mathbb{R}_+$ and $\lambda(\Gamma) \stackrel{\mathrm{def}}{=} (4\Gamma)/h \gg 1$. However, when $0 \leqslant \lambda \lesssim 1$, the exponential-decay strategy can outperform the power-law strategy in terms of entropic speed. In Fig. 2 we plot the constant values of the entropic speed v_{E} and the entropic efficiency η_{E} that emerge from the particular parametric expression of $\mathcal{F}(\theta)$. The expression of the Fisher information, in turn, depends on the particular su(2; $\mathbb{C}$) Hamiltonian model considered. More formally, combining Eqs. (22) and (25), we get $v_{\mathrm{E}}^{(\text{power-law})}(\Gamma) = [e^{\lambda\theta_0}/(1+\lambda\theta_0)^2]v_{\mathrm{E}}^{(\text{power-law})}(\Gamma)$. Introducing the function $f_{\mathcal{P}}(\lambda,\theta_0) \stackrel{\mathrm{def}}{=} e^{\lambda\theta_0}/(1+\lambda\theta_0)^2$, the two-dimensional parametric region $\mathcal{P}$ where the exponential law decay strategy yields entropic speed values higher than those of the power law decay strategy is given by

TABLE III. Schematic behavioral description of the entropy production rate, speed, and Fisher information in the selected four su(2; $\mathbb{C}$) Hamiltonian models. In particular, for each model, we point out the Grover-like or fixed-point-like property exhibited by its corresponding analog quantum search algorithm.

Analog quantum search	su(2; $\mathbb{C}$) Hamiltonian model	Fisher information	Speed	Entropy production rate
Grover-like	Constant $B_\perp$, original	Constant	Higher	Higher
Grover-like	Oscillating $B_\perp$, generalized	Oscillatory	High	High
Fixed-point-like	Power law decay of $B_\perp$, generalized	Power law decay	Low	Low
Fixed-point-like	Exponential decay of $B_\perp$, generalized	Exponential decay	Lower	Lower

$\mathcal{P} \stackrel{\text{def}}{=} \{(\lambda, \theta_0) \in \mathbb{R}_+ \times \mathbb{R}_+ : f_{\mathcal{P}}(\lambda, \theta_0) < 0\}$. A plot of such a region $\mathcal{P}$ appears in Fig. 3. We emphasize that, for values of the parameter λ sufficiently large, the power law decay strategy outperforms the exponential decay strategy in terms of entropic speed. To have a physical grasp of a typical value of λ, we recall that $\lambda = (4\Gamma)/h$ and $\Gamma = (|e|\hbar B_\perp)/2mc$. Therefore, assuming to consider a magnetic field with initial intensity $B_\perp$ of the order of 0.2 T (a value typical of neodymium magnets), $\lambda \simeq 37$ [MKSA]. Furthermore, in Table III we summarize the behavior of the entropy production rate r_{E}, the entropic speed v_{E}, and the Fisher information $\mathcal{F}(\theta)$ for each of the four quantum mechanical evolutions considered. Finally, for each quantum evolution, we specify the type of continuous-time quantum search it resembles.

V. CONCLUSIONS

In this article, we presented an information geometric characterization of entropic speeds and entropy production rates that emerge from the geodesic motion on manifolds of parametrized quantum states. These pure states emerge as outputs of suitable su(2; $\mathbb{C}$) time-dependent Hamiltonian evolutions employed to specify distinct types of continuous-time quantum search schemes. The Riemannian metrization on the manifold is essentially specified by the Fisher information evaluated along the parametrized squared probability amplitudes obtained from the analysis of the quantum mechanical temporal evolution of a spin-1/2 particle in an external time-dependent magnetic field that prescribes the su(2; $\mathbb{C}$) Hamiltonian model. In Fig. 1, we show the manner in which a specific Fisher information behavior arises from a given su(2; $\mathbb{C}$) Hamiltonian model characterized by a particular magnetic field configuration (see Table II). We use a minimum action principle to transfer a quantum system from an initial state to a final state on the manifold in a finite temporal interval. Furthermore, we demonstrate that the minimizing (optimum) path is the shortest (geodesic) path between the two states and, in particular, also minimizes the total entropy production, that is, the thermodynamic divergence of the path that occurs during the transfer. Then, by evaluating the entropic speed and the total entropy production along the optimum transfer paths in the four chosen physical scenarios of interest in analog quantum search problems, we demonstrate in a clear quantitative manner that to a faster transfer there necessarily corresponds a higher entropy production rate (see Fig. 2 and Table III). Thus we conclude that lower (entropic) efficiency values do appear to accompany higher (entropic) speed values in quantum transfer processes. In particular, quantum mechanical evolutions that generate probability paths with a Fisher information that exhibits an exponential decay behavior seem to achieve the highest entropic efficiency with the cost of also having the lowest entropic speed. By contrast, probability paths with a constant Fisher information appear to be the fastest but also the most inefficient from an entropic standpoint. A graphical summary of these results, including all four su(2; $\mathbb{C}$) Hamiltonian models considered in this paper (see Table II), appears in Fig. 2 and Table III.

In conclusion, we view our investigation presented in this paper as a natural progression of our works presented in Refs. [14,16]. It constitutes a nontrivial preliminary effort toward understanding quantum search algorithms from a thermodynamical perspective developed within an information geometric setting. It is our intention to improve upon the analysis provided in this paper and pursue these fascinating lines of investigations in forthcoming scientific efforts. Of course, it is our sincere hope that our work will inspire other scientists to further explore these research avenues in the near future.

ACKNOWLEDGMENTS

C.C. is grateful to the United States Air Force Research Laboratory (AFRL) Summer Faculty Fellowship Program for providing support for this work. Any opinions, findings, and conclusions or recommendations expressed in this manuscript are those of the authors and do not necessarily reflect the views of AFRL.

[1] L. K. Grover, Phys. Rev. Lett. **79**, 325 (1997).
[2] M. A. Nielsen and I. L. Chuang, *Quantum Computation and Information* (Cambridge University Press, Cambridge, UK, 2000).
[3] J. J. Alvarez and C. Gomez, arXiv:quant-ph/9910115.
[4] A. Miyake and M. Wadati, Phys. Rev. A **64**, 042317 (2001).
[5] C. Cafaro and S. Mancini, in *31st International Workshop on Bayesian Inference and Maximum Entropy Methods in Science and Engineering*, edited by P. Goyal, A. Giffin, K. H. Knuth, and E. Vrscay, AIP Conf. Proc. No. 1443 (AIP, Melville, NY, 2012), p. 374.
[6] C. Cafaro and S. Mancini, Physica A (Amsterdam) **391**, 1610 (2012).
[7] C. Cafaro, Physica A (Amsterdam) **470**, 154 (2017).
[8] C. H. Bennett, Int. J. Theor. Phys. **21**, 905 (1982).
[9] J. M. R. Parrondo, J. M. Horowitz, and T. Sagawa, Nat. Phys. **11**, 131 (2015).
[10] C. Cafaro and P. van Loock, in *32nd International Workshop on Bayesian Inference and Maximum Entropy Methods in Science and Engineering*, edited by U. von Toussaint, AIP Conf. Proc. No. 1553 (AIP, Melville, NY, 2013), p. 275.
[11] C. Cafaro and P. van Loock, Physica A (Amsterdam) **404**, 34 (2014).
[12] R. Beals, S. Brierley, O. Gray, A. W. Harrow, S. Kutin, N. Linden, D. Shepherd, and M. Stather, Proc. R. Soc. A **469**, 20120686 (2013).
[13] R. Perlner and Y.-K. Liu, arXiv:1709.10510.
[14] C. Cafaro and P. M. Alsing, Phys. Rev. E **97**, 042110 (2018).
[15] T. Byrnes, G. Forster, and L. Tessler, Phys. Rev. Lett. **120**, 060501 (2018).
[16] C. Cafaro and P. M. Alsing, Int. J. Quantum Inf. **17**, 1950025 (2019).
[17] C. Cafaro and P. M. Alsing, Phys. Scr. **94**, 085103 (2019).
[18] T. M. Cover and J. A. Thomas, *Elements of Information Theory* (John Wiley & Sons, Inc., New York, 2006).
[19] B. R. Frieden, *Physics from Fisher Information* (Cambridge University Press, Cambridge, NY, 1998).

[20] S. Amari and H. Nagaoka, *Methods of Information Geometry* (Oxford University Press, Oxford, 2000).
[21] S. L. Braunstein, C. M. Caves, and G. J. Milburn, Ann. Phys. (NY) **247**, 135 (1996).
[22] S. L. Braunstein and C. M. Caves, Phys. Rev. Lett. **72**, 3439 (1994).
[23] G. E. Crooks, http://threeplusone.com/sher.
[24] F. Weinhold, J. Chem. Phys. **63**, 2479 (1975).
[25] G. Ruppeiner, Phys. Rev. A **20**, 1608 (1979).
[26] P. Salamon, J. Nulton, and E. Ihrig, J. Chem. Phys. **80**, 436 (1984).
[27] P. Salamon and R. S. Berry, Phys. Rev. Lett. **51**, 1127 (1983).
[28] P. Salamon, J. D. Nulton, and R. S. Berry, J. Chem. Phys. **82**, 2433 (1985).
[29] G. E. Crooks, Phys. Rev. Lett. **99**, 100602 (2007).
[30] F. De Felice and J. S. Clarke, *Relativity on Curved Manifolds* (Cambridge University Press, Cambridge, UK, 1990).
[31] L. Diosi, K. Kulacsy, B. Lukacs, and A. Racz, J. Chem. Phys. **105**, 11220 (1996).
[32] G. M. Rotskoff, G. E. Crooks, and E. Vanden-Eijnden, Phys. Rev. E **95**, 012148 (2017).
[33] E. P. Gyftopoulos and G. P. Beretta, *Thermodynamics: Foundations and Applications* (Dover Publications, Inc., Mineola, NY, 2005).
[34] J. Anandan and Y. Aharonov, Phys. Rev. Lett. **65**, 1697 (1990).
[35] J. J. Sakurai, *Modern Quantum Mechanics* (Addison-Wesley Publishing Company, Inc., Redwood City, CA, 1994).
[36] C. Cafaro and S. Mancini, Phys. Rev. A **82**, 012306 (2010).
[37] C. Cafaro and P. van Loock, Phys. Rev. A **89**, 022316 (2014).
[38] A. Messina and H. Nakazato, J. Phys. A **47**, 445302 (2014).
[39] R. Grimaudo, A. S. M. de Castro, H. Nakazato, and A. Messina, Ann. Phys. (Berlin) **530**, 1800198 (2018).